Mathematical Model for the Nonsteady Decomposition of Intumescent Coatings

Colomba Di Blasi and Carmen Branca
Dipartimento di Ingegneria Chimica, Universitá degli Studi di Napoli "Federico II," 80125 Napoli, Italy

A 1-D transient mathematical model was studied for a composite system consisting of a substrate (steel) and an intumescent coating exposed to radiative heating. By applying a simple heat conduction equation for the first material, a general model proposes the coating consisting of three components, which degrade according to independent finite-rate reactions. Mass and heat transfer take place across a variable volume medium, including a simplified mechanism for bubble dynamics and material swelling. A parametric analysis clarifies the role of several parameters on the fire retardancy performance of the coating. Good agreement is obtained between predictions and measurements of the substrate temperature profiles.

Introduction

Intumescent materials are applied (Kandola et al., 1997) in the form of coatings for the surface of substrates (Cagliostro et al., 1975; Anderson et al., 1988) or as additives during polymer preparation prior to fabrication into a product (Camino et al., 1984; Siat et al., 1998). When exposed to heat, these materials undergo swelling with the formation of cellular char. This behavior, indicated as intumescence, is a condensed phase mechanism of flame retardancy (Weil et al., 1996; Horrocks, 1996; Lewin, 1998), because char formation reduces material flammability first by reducing the amount of volatiles generated. In addition, the char layer acts as a physical barrier which greatly reduces heat transfer to the underlying virgin material and hinders, on the one hand, the passage of combustible volatiles and molten polymer towards the flame and, on the other hand, oxygen diffusion inside the solid.

Usually, three basic components are employed in the synthesis of intumescent materials: a catalyst, a charring material, and a swelling/blowing agent (Weil et al., 1996; Horrocks, 1996; Lewin, 1998). During degradation, a viscoelastic phase is formed, followed by swelling and charring, both of which should be properly synchronized (Anderson et al., 1998). Devolatilization (blowing agent) should not occur before a viscoelastic state is attained, so that the volatiles are trapped in the form of bubbles, but should be completed before significant solidification (charring) of the material takes place. Properties, in particular, viscosity, of the molten phase are important in relation to both swelling and char characteristics. For instance, if the molten viscosity is too high, swelling does not occur. On the hand, if it becomes too low, large cells are formed during the swelling process and the resulting char may be very frangible, so losing its insulation properties.

Given the low environmental impact, a great deal of activity is under way on the development and testing of intumescent materials (a collection of articles regarding this sector is reported in Le Bras et al., 1998). It can be understood that the interaction between chemistry and transport phenomena plays a key role in effecting intumescent behavior. Hence, transport models could be useful tools for synthesizing intumescent materials and predicting their reaction to fire. However, a recent review (Di Blasi, 2000a), shows that only very simplified descriptions of physical processes based on a one-dimensional enthalpy equation coupled with different relations for volume variation are available (Cagliostro et al., 1975; Anderson and Wauters, 1984; Buckmaster et al., 1986; Mameleev and Gibov, 1998).

All the transport models of intumescent systems have been applied for coatings and very limited model sensitivity analysis and validation have been carried out. In particular, predictions of the process dynamics in terms of the main variables of interest (temperatures, chemical species, velocity, sample volume) have never been presented, apart from the time evolution of the substrate temperature. Such predictions are qualitatively sound, but no quantitative agreement is

Correspondence concerning this article should be addressed to C. Di Blasi.

shown with measurements unless strong alterations in the coating thermal conductivity and kinetic constants (and reaction energetics) are introduced (Cagliostro et al., 1975), or a large shift in time is made to match theory with experiments (Anderson and Wauters, 1984). Nonetheless, agreement is still fair, especially for high temperatures. Despite the industrial interest in the use of intumescent additives in synthetic polymers, experimental data needed for the formulation and the application of mathematical models are not yet available, that is, input parameters (physical properties and reaction kinetics) and measurements for model validation (for instance, temperature profiles for conditions where both transport phenomena and chemical kinetics are important).

The failure of the current intumescent coating models to give quantitative predictions and the lack of sufficient data for intumescent polymers have motivated the use of the system considered by Cagliostro et al. (1975) as a starting point for this study, the purpose of which is to present a more advanced model for intumescent systems. It couples the degradation dynamics of three components with the basic transport equations written for a 1-D variable-volume system including a simplified bubbling mechanism. It is shown that this more accurate description of physical and chemical processes allows quantitative agreement to be obtained between the predicted and the measured substrate temperature profiles. Furthermore, a parametric analysis, carried out in order to clarify the influences of the main parameters and model assumptions on the thermal response of the system, indicates that coating size (swelling and initial thickness) and radiative heat transfer across the highly porous char are the predominant factors for the substrate thermal response.

The Problem

The 1-D composite system of interest is formed by a substrate of thickness τ_s and an intumescent coating of initial thickness τ_{c0} $(t = 0)$, whose upper surface is exposed to radiative heating. For a given instant $(t > 0)$, three zones appear along the coating thickness, that is, the virgin, the reaction, and the reacted zone (Figure 1). Along the virgin zone, the temperature is too low for any significant chemical or physical transformation. In the reaction zone, the material decomposes into small amounts of volatiles and a molten phase intermediate. When the temperature is further increased, the molten phase begins to evaporate and gas bubbles appear, which, on dependence of the molten properties, grow and cause swelling. Indeed, for even higher temperatures, solidification of the swollen material is observed, so that the reacted zone consists of a cellular char structure.

Chemical Reactions

The chemistry of the intumescent material is the same as that proposed by Cagliostro et al. (1975). The material consists of three components, S_1, S_2 and S_3, present in proportions Y_{10}, Y_{20} and Y_{30}, which degrade according to three independent reactions

$$S_1 \xrightarrow{k_1} V_1,\ S_2 \xrightarrow{k_2} V_2,\ S_3 \xrightarrow{k_3} \nu_c C + \nu_v V_3 \qquad \text{(r1–r3)}$$

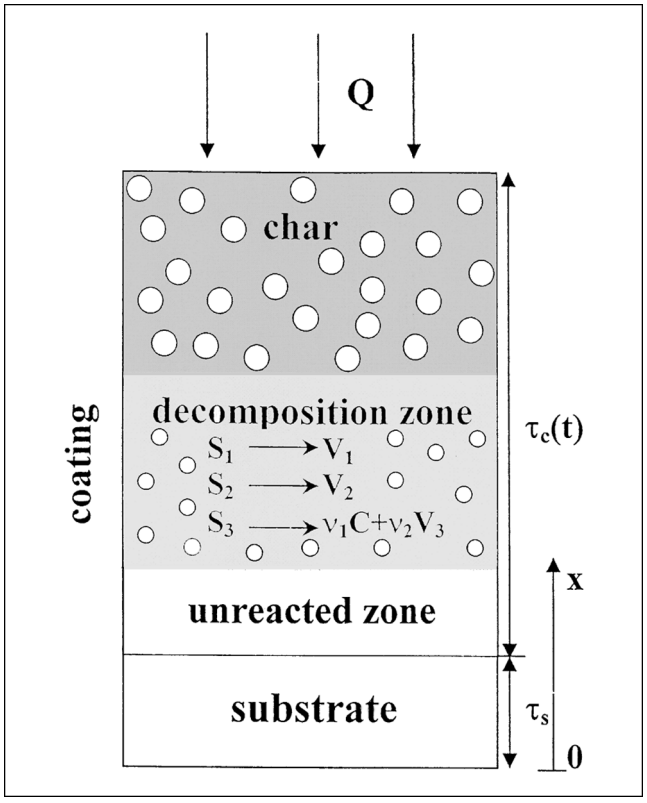

Figure 1. 1-D substrate/intumescent coating system.

corresponding to melting (with volatile release), swelling and charring (again with some volatile release), respectively. V_1, V_2, and V_3 are lumped volatile species and C is the charred solid residue. The experimental weight-loss curve reported by Cagliostro et al. (1975) (heating rate $6K$/min) has been used to estimate the kinetic parameters for reactions r1–r3, through numerical solution of the conservation equations for the condensed-phase species and a direct method to minimize the objective function. The new set of kinetic constants is, in practice, coincident with that reported by Cagliostro et al. (1975), including a second-order rate for component S_2, probably owing to the global character of the reaction mechanism. Hence, this (Table 1) is used here to facilitate the comparison with previous published simulation results. It is worth noting that the occurrence of intumescence is related to the material properties through the temperature interval where the decomposition of the component S_2 takes place, but the process should be defined by further assumptions.

Mathematical Description of Transport Phenomena

The chemistry of reactions r1–r3 should be coupled with the description of transport phenomena. Compared with the thermal model by Cagliostro et al. (1975), where the effects of volume variations, described by means of an empirical relation, were simply treated in terms of an "effective" thermal conductivity for the enthalpy conservation equation, a general formulation is presented here of the finite-difference equations for heat and mass transport for systems with variable volume.

Table 1. Kinetic Constants and Physical Properties of Coating and Substrate*

Kinetic Constants and Reaction Enthalpies		Physical Properties	
A_1 (s^{-1})	800 (+)	c_c (kJ/kg·K)	1.884 (+)
E_1 (kJ/mol)	53.384 (+)	c_f (kJ/kg·K)	1.63 (+)
A_2 (s^{-1})	6.9×10^5 (+)	c_s (kJ/kg·K)	0.42 (+)
E_2 (kJ/mol)	93.035 (+)	c_g (kJ/kg·K)	1.00 (+)
A_3 (s^{-1})	5.0 (+)	ϵ_{c0}	0.30 (*)
E_3 (kJ/mol)	63.786 (+)	λ_{c0} (kW/m·K)	0.345×10^{-3} (+)
ν_C	0.784 (+)	λ_f (kW/m·K)	0.067×10^{-3} (+)
ν_G	0.216 (+)	λ_s (kW/m·K)	37.68×10^{-3} (+)
Δh_1 (kJ/kg)	−1256(*)	ρ_{c0} (kg/m^3)	1400 (+)
Δh_2 (kJ/kg)	−1256(*)	e_{c0}	1.00 (+)
Δh_3 (kJ/kg)	9789(+)	e_f	0.80 (+)
Y_{10}	0.28(+)	d_{c0} (m)	5.00×10^{-6}(*)
Y_{20}	0.17(+)	d_f (m)	325.0×10^{-6}(*)
Y_{30}	0.55(+)	E	3.00(*)
		β	1.00(*)
		W_{V2}, W_g (kg/mol)	30×10^{-3}(*)
		ω	1(*)
		h (kW/m^2)	20(*)
		Q (kW/m^2)	157
		τ_{c0} (m)	0.2×10^{-2}
		τ_s (m)	0.15×10^{-2}

*Values obtained from Cagliostro et al. (1975) (+) or estimated in this study (*).

The coating is discretized into a number (n) of elementary cells, as shown in Figure 2, of volume $V_i = A\Delta x_i$, where A is the (constant) cross section and Δx_i is the (variable) size of the cell along the coating thickness. With reference to the elementary volume V_i, for a generic variable ϕ (for instance, the density of volatile species), the conservation equation can be written as

$$\frac{\partial \epsilon_i V_i \phi_i}{\partial t} = A(W_{i-1}\phi_{i-1} - W_i\phi_i) + A(N_{i-1} - N_i) + V_i\delta_i, \qquad i = 1, n \quad (1a)$$

where W and N are the convective and diffusive mass flux, respectively, and δ is the sink/source term. The first contribution on the right-hand side is the convective transport, the second is the diffusive transport, and the third is the net production. The final form of the equation is then

$$\frac{1}{\Delta x_i}\frac{\partial \epsilon_i \Delta x_i \phi_i}{\partial t} = -\frac{(W_i\phi_i - W_{i-1}\phi_{i-1})}{\Delta x_i} + \frac{(N_{i-1} - N_i)}{\Delta x_i} + \delta_i, \qquad i = 1, n \quad (1b)$$

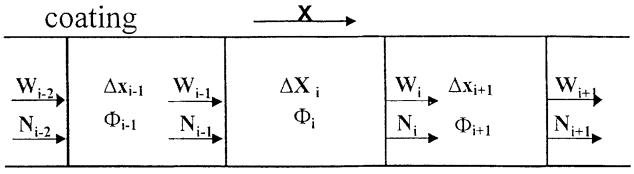

Figure 2. Finite difference discretization of the computational domain for the coating.

The accumulation term can be expressed as

$$\frac{1}{\Delta x_i}\frac{\partial \epsilon_i \Delta x_i \phi_i}{\partial t} = \frac{\partial \epsilon_i \phi_i}{\partial t} + \frac{\epsilon_i \phi_i}{\Delta x_i}\frac{\partial \Delta x_i}{\partial t} \quad (2)$$

where the second contribution at the righthand side is formally equivalent to convective transport. Given the increase in the volume, it has a negative effect for the accumulation of the conserved variable (that is, concentrations or temperatures tend to become lower because of this effect). In addition, the increase in the size of the spatial cell, as a consequence of the swelling process, causes lower fluxes and consequently, lower spatial gradients of the conserved variable.

In the formulation of the conservation equations for the condensed-phase species it is assumed that the related mass is always associated with the same elementary control volume. Thus, though the apparent species density varies as a consequence of the swelling process (volume variation), conservation equations in terms of mass fractions (Y_1, Y_2, Y_3, Y_C) should only account for the net generation due to chemical reactions

$$\frac{\partial Y_1}{\partial t} = -K_1Y_1, \quad \frac{\partial Y_2}{\partial t} = -K_2Y_2^2, \quad \frac{\partial Y_3}{\partial t} = -K_3Y_3, \quad \frac{\partial Y_C}{\partial t} = \nu_c K_3 Y_3 \quad (3\text{–}6)$$

where

$$K_j = A_j \exp(-E_j/RT), \quad j = 1,3 \quad (7a\text{–}7c)$$

(Equations 3–6 should be written for each elementary cell.)

In order to specify the mathematical model for this problem, some assumptions are made in the treatment of the convective transport and the swelling (bubbling) process. The rate of viscous flow through the charred zone takes place without significant overpressure, given the large void fraction (permeability depends on the third-order power of porosity (Collins, 1961). Mass transfer of the volatiles inside the degrading region also occurs at a constant pressure (but with volume variation) and includes vapor accumulation in the form of bubbles. More precisely, while the volatiles evolving from the component S_1 and S_3 leave the degrading material instantaneously, part of the volatile mass produced by the components S_3 gives rise to the formation of bubbles, which occupy a volume computed according to the ideal gas law (given a certain temperature). Local release of bubble volatiles takes place only when complete degradation of the component S_2 has occurred (Yang et al., 1995). During solidification (charring), the pressure usually grows with rupture of the bubble walls. Bubbles roughly maintain their shape (volume) which, however, becomes open and the pressure lowers to ambient values (Mamleev and Gibov, 1998). In order to simplify the mathematical description of the problem, the effects of the momentaneous overpressure are again neglected. As will be shown, this simplified bubbling mechanism requires only one or two empirical parameters, whose role on process dynamics

and characteristics will be assessed through a sensitivity analysis.

In addition to the condensed-phase mass conservation equations (Eqs. 3–6), equations are also needed for the volume (per unit surface) occupied by bubbles Δ_b, and condensed phase Δ_{ls}, (the total cell volume and the void fractions are determined in consequence), the total gas density ϱ, the gas velocity u, and the temperature T (the solid, molten and vapor phases are assumed to be in thermal equilibrium, as the condensed phase volumetric heat capacity is much larger than that of the gas phase (Ellard, 1973)). If the densities of the gas-phase species are also required, further mass conservation equations should be considered.

For each elementary control volume, the bubble volume (per unit surface) Δb_i is obtained from the state equation, where the partial pressure of the volatile component V_2 is assumed to be at the atmospheric value

$$A\Delta b_i = \beta \frac{M_0(Y_{20} - Y_{2i})\,\Re T_i}{P_0 W_{V2}} (\Delta x_i \le E\Delta x_0), \quad i = 1, n \quad (8)$$

It can be observed that no bubbles are present until the degradation of S_2 begins ($Y_{2i} = Y_{20}$). Successively, the bubble volume increases because of the increase in both the amount of volatiles evolved and the temperature. The parameter β is empirical and accounts for the partial contribution of the volatiles evolved from component S_2 in the swelling process. If a further empirical parameter E (expansion factor) is introduced to limit the maximum volume expansion, successively higher values of β can be used to make the swelling process faster. It is also assumed that the volume occupied by the condensed phase decreases in proportion to the devolatilized mass

$$\Delta_{lsi} = (1 - \epsilon_{c0})\Delta_{ls0}(Y_{1i} + Y_{2i} + Y_{3i} + Y_{ci}), \quad i = 1, n \quad (9)$$

and consequently the total cell size and void fraction can be expressed as

$$\Delta x_i = \Delta x_0 + \Delta b_i \quad (\Delta x_i \le E\Delta x_0), \quad \epsilon_i = \frac{\Delta b_i + \Delta x_0 - \Delta_{lsi}}{\Delta x_i}, \quad i = 1, n \quad (10\text{–}11)$$

The total volatile density ϱ is obtained from the state equation as

$$\varrho_i = \frac{W_g P_0}{\Re T_i}, \quad i = 1, n \quad (12)$$

The total continuity equation is used to evaluate the gas velocity u and is expressed as

$$\frac{1}{\Delta x_i}\frac{\partial \epsilon_i \Delta x_i \varrho_i}{\partial t} = -\frac{(u_i \varrho_i - u_{i-1}\varrho_{i-1})}{\Delta x_i} + \omega_i, \quad i = 1, n \quad (13)$$

where ω_i, the production term, is due to the devolatilization of the three components

$$\omega_i = -\frac{M_0}{A\Delta x_i}\left(\frac{\partial Y_{1i}}{\partial t} + \frac{\partial Y_{3i}}{\partial t}\right) + \frac{M_{bi}}{A\Delta x_i}, \quad i = 1, n \quad (14)$$

Particular care is needed for the definition of M_b, that is, the rate of volatile production responsible for the bubbling. In the first stage, when swelling is under way, it is expressed as

$$M_{bi} = M_0(1 - \beta)\frac{\partial Y_{2i}}{\partial t} (Y_{2i} \ge 0, \quad \Delta x_i < E\Delta x_0) \quad (15a)$$

For longer times, volatiles produced from the decomposition of S_2 in excess with respect to the amount necessary to attain the maximum expansion for a given cell are instantaneously released

$$M_{bi} = M_0 \frac{\partial Y_{2i}}{\partial t} (Y_{2i} \ge 0, \Delta x_i = E\Delta x_0) \quad (15b)$$

Finally, when decomposition of the component S_2 is completed, volatiles retained by the material during the swelling process are also released and M_b is expressed as

$$M_{bi} = M_0\left(\sum_j \beta \frac{\partial Y_{2i}}{\partial t}\right)_{j=1,n_b} (Y_{2i} = 0, \Delta x_i = E\Delta x_0) \quad (15c)$$

where j is the time index and varies from 1 ($t = \Delta t$) to n_b for the time ($t = n_b\Delta t$) corresponding to the attainment of the maximum cell size.

Assuming that volatile species V_1, V_2 and V_3 present the same properties, the enthalpy conservation equation can be written as

$$\frac{M_0}{A}\frac{\partial(Y_{1i}h_{1i} + Y_{2i}h_{2i} + Y_{3i}h_{3i} + Y_{Ci}h_{Ci})}{\partial t} + \frac{\partial \varrho_i \epsilon_i \Delta x_i h_{gi}}{\partial t} = (\varrho_{i-1}u_{i-1}h_{gi-1} - \varrho_i u_i h_{gi}) + (q_{i-1} - q_i) + \frac{M_0}{A}\sum_j \Delta h_j\left(\frac{-\partial Y_{ji}}{\partial t}\right), \quad q_i = -\lambda_i^* \frac{\partial T_i}{\partial x}, \quad i = 1, n \quad (16,17)$$

where $h_{ji} = c_j T_i$, $j = 1, 2, 3, C$ and $h_{gi} = c_g T_i$.

The effective thermal conductivity is described according to the model specifically developed for intumescent coatings by Anderson et al. (1988)

$$\lambda^* = \frac{\lambda_{c0}\lambda_g}{(1 - \epsilon)\lambda_g + \epsilon\lambda_{c0}} \quad (18)$$

For low porosities (and conversion), the medium thermal conductivity is nearly the same as that of the virgin coating, and as the porosity increases (high conversion and swelling), it approaches that of the gas (volatiles). However, given the high porosity of char and the high temperatures of fire-level heat fluxes, radiative heat transfer may become very important. Therefore, the model given by Anderson et al. (1988) has been extended to include a radiative contribution expressed as (Di Blasi, 1996a)

$$\lambda^* = \frac{\lambda_{c0}\lambda_g}{(1-\epsilon)\lambda_g + \epsilon\lambda_{c0}} + 13.5\sigma T^3 \frac{d_c}{\epsilon\omega} \qquad (19)$$

where

$$d_c = d_{c0}(1-\eta) + d_f\eta, \quad \eta = \frac{Y_C}{\nu_c Y_{30}} \qquad (20a\text{–}20b)$$

The gas thermal conductivity is a function of temperature (Di Blasi, 2000b)

$$\lambda_g = 4.815\times10^{-7}T^{0.717} \qquad (21)$$

For comparison purposes, two further models for the effective thermal conductivity applied for charring materials are also considered. In the first, a linear variation is assumed between the virgin material and the final char values (mixture rule) as in Di Blasi and Wichman (1995) and Di Blasi (1996b)

$$\lambda^* = (1-\epsilon)\lambda_c + \epsilon\lambda_g,\ \lambda_c = \alpha\lambda_{c0} + (1-\alpha)\lambda_f,\ \alpha = Y_1 + Y_2 + Y_3 \qquad (22a,\ 22b\text{–}23)$$

In the other model (Curtis and Miller, 1988), a dependence on the porosity is again assumed

$$\lambda^* = \lambda_{c0}\left(\frac{\lambda_g}{\lambda_{c0}}\right)^{\epsilon} \qquad (24)$$

The substrate is an inert, nonporous material and the only process of interest is unsteady, 1-D heat conduction through a constant volume (and property) medium

$$c_s\varrho_s\frac{\partial T_s}{\partial t} = \lambda_s\frac{\partial}{\partial x}\left(\frac{\partial T_s}{\partial x}\right) \qquad (25)$$

which can easily be approximated into a finite difference formulation.

The partial differential equations for the degrading coating and the inert substrate are coupled by boundary conditions at the interface ($x = \tau_s$)

$$\varrho_g u = 0, \quad T_s = T, \quad \lambda_s\frac{\partial T_s}{\partial x} = \lambda^*\frac{\partial T}{\partial x} \qquad (26\text{–}28)$$

which correspond to the impermeability, the continuity of temperature between the two media, and the heat flux balance, respectively. Other boundary conditions are also needed. At the bottom surface, the substrate is thermally insulated, that is, a condition of zero heat flux is imposed (Cagliostro et al., 1975). At the upper surface, heating is described by a heat flux balance which accounts for external heat radiation (Q), surface re-radiation and convective cooling

$$\lambda^*\frac{\partial T}{\partial x} = h(T_e - T) + \sigma(1-e)\left(T_e^4 - T^4\right) + eQ,$$
$$e = (1-\eta)e_{c0} + \eta e_f \qquad (29\text{–}30)$$

The system of differential equations is approximated by finite differences and the solution is handled by an operator-splitting method originally proposed by Yanenko (1971) and whose validity in the numerical simulation of reactive systems has been already ascertained (Wichman, 1991). The production terms and the effects of volume variation (ordinary differential equations) are afforded by the implicit Euler method, whereas transport phenomena are treated by the implicit hybrid scheme (Patankar, 1980). This scheme, applied to convection/diffusion equations, guarantees stability, convergence, and consistency of the numerical solution. Accuracy is also guaranteed by a proper selection of the space and time discretization steps. It is also worth noting that the swelling of each elementary control volume of the integration domain does not introduce any particular obstacle in the computation of the solution as, contrary to the case of moving boundary Stefan problems (Carlslaw and Jaeger, 1980), the boundary is not associated with a predefined value of a process variable (for instance, temperature). On the other hand, the numerical solution of finite difference systems with variable grid is not critical in terms of accuracy (Patankar, 1980).

Results

As a reference case, a composite system coating/substrate is examined with properties (Table 1) in large part derived from Cagliostro et al. (1975). They are representative of steel (substrate) and a coating specifically developed for aerospace applications. The heating conditions again reproduce those used by Cagliostro et al. (1975), with a radiative heat flux of 157 kW/m^2, $\tau_{c0} = 0.2\times10^{-2}$m, and $\tau_s = 0.15\times10^{-2}$m. The volume expansion factor E for coatings used in the aerospace industry is reported to vary in the range 1–9 (Anderson et al., 1988), and a value of 3 with $\beta = 1$ is chosen for the reference case.

Simulations have been made by varying model parameters, such as E and β (bubble mechanism), the coating thickness, and the thermal conductivity model, whereas a sensitivity analysis is given for the coating properties and the kinetic constants of the degradation reactions r_1–r_3. Finally, comparisons are made of the predicted and measured (Cagliostro et al., 1975) substrate temperature profiles on the dependence of time. All the simulations have been carried out with a time step of 5×10^{-4}s and initial space steps of 8×10^{-6}m, giving grid-independent solutions for the reference case.

Process Dynamics

Details of time and space evolution of the variables of interest are given as simulated by the previously introduced conservation equations with the effective thermal conductivity model proposed by Anderson et al. (1988) including the radiative contribution (Eq. 19, in the following indicated as model A). The heating dynamics of the substrate (reference

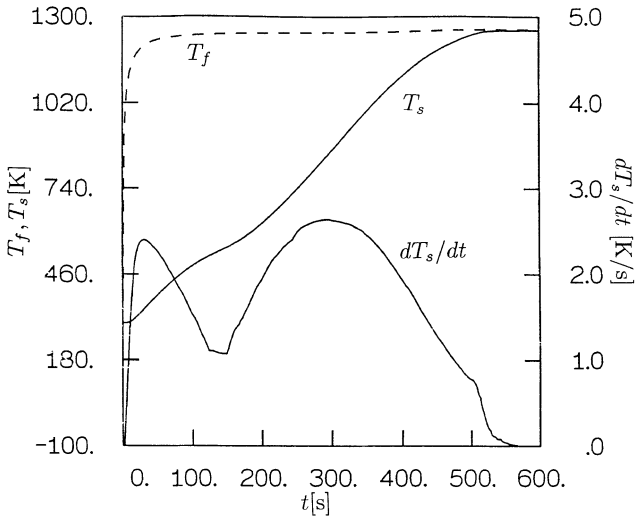

Figure 3. Time profiles of substrate temperature T_s, temperature of coating at irradiated surface, T_f, and time derivative of the substrate temperature.

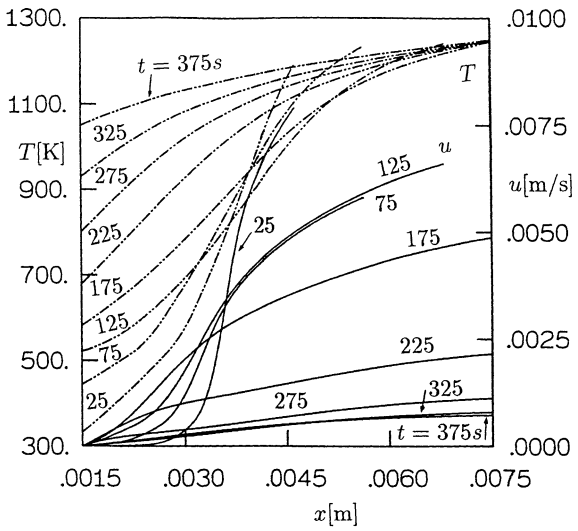

Figure 5. Temperature T (dashed-dotted lines) and velocity u (solid lines) profiles along variable coating thickness for several times.

case) are shown in Figure 3 by means of the profiles of the substrate temperature at the coating/substrate interface and its time derivative (the temperature of the substrate is spatially uniform; thus, the interface evolution is representative of the thermal history of the substrate at all locations). For comparison purposes, the time profile of the coating temperature at the surface T_f is also shown. The characteristics of volatile formation are shown in Figure 4, through the time profiles of the global devolatilization rates (dY_{VT}/dt and dY_{VkT}/dt, $k = 1,3$, respectively, where the total coating mass fraction Y_T refers to all the components and Y_{kT} refers to each of the three components). The process roughly consists of three stages. In the first, which lasts about 27 s, the mass loss is negligible and the substrate heating rate attains a maximum (indicated in the following as d_1) of about 2.4 K/s. In the second stage, a decrease in the substrate heating rate is followed by a region characterized by an almost constant value (times shorter than 143 s). The duration of the second stage (116 s), indicated in the following as delay time t_d is also delimited by the two local maxima in the global coating devolatilization rate and gives rise to a mass loss of about 50% (of the initial coating mass). The dynamics of component evolution (Figure 4) shows that their degradation occurs simultaneously, but a large amount of the volatile mass evolved in this stage is essentially due to decomposition of S_1 and S_2. Finally, in the third stage, a new increase in the substrate heating rate is observed with a maximum (indicated in the following as d_2) of about 2.6 K/s and the attainment of steady conditions. In this stage, the slow devolatilization rates are associated with small amounts of volatiles evolved, mainly as a consequence of the decomposition of component S_3. As expected, heating rates at the coating surface are very high (up to 250 K/s).

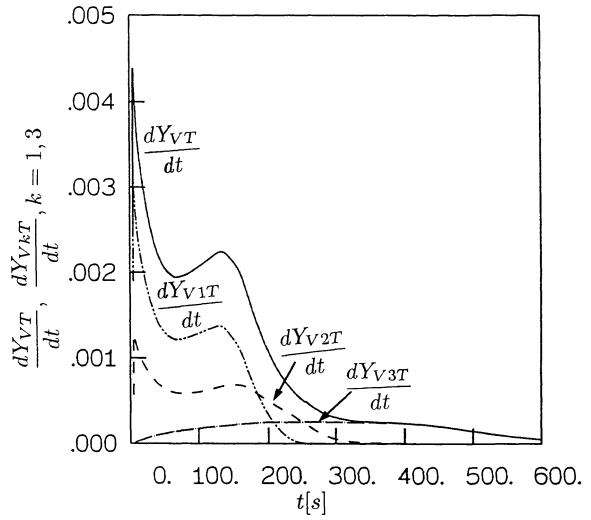

Figure 4. Time profiles of global (dY_{VT}/dt) and component (dY_{VkT}/dt, $k = 1, 3$) volatile formation rate.

The time evolution of temperature and gas velocity along the coating thickness (reference case) is shown through Figure 5. The high value of the applied radiation intensity results in temperatures sufficiently high for the onset of the degradation process at very short times at least for a superficial coating layer. In accordance with the degradation kinetics, the degradation of components S_1 precedes that of the components S_2, which, in turn, precedes that of component S_3 (not shown). Given the presence of high-temperature gradients along the coating thicknesses, as already observed in Figure 4, the degradation of the three coating components occurs simultaneously, although maximum rates are observed at different, time-dependent, spatial locations.

The first and second process stages are characterized by very high spatial temperature gradients and large gas velocities (high coating devolatilization rates). Coating expansion is a very fast process and is practically completed in a time of 151 s, when about 26% of the component S_2 is not yet de-

volatilized. Its duration is slightly longer than that corresponding to the first and second stages of substrate heating. The high spatial temperature gradients during the initial process transients are due, above all, to coating swelling which makes inward heat transfer from the heated surface more difficult. Indeed, a continuous reduction in the first contribution of the effective thermal conductivity (Eq. 19) is observed, associated with an increase in the medium porosity. In the second place, during these initial stages, a large quantity of volatiles is released and the convective transport of hot gases from the degrading coating results in a significant cooling effect.

The third slow stage corresponds essentially to solidification (charring) of the swollen coating with temperatures along the composite system approaching the surface value. In this process stage (times longer than 143 s), gas velocities are rapidly reduced and heat transfer takes place across a constant volume medium. The high temperatures and porosities attained along the upper part of the charred coating make the radiative contribution in the effective thermal conductivity large, so that spatial temperature gradients are rapidly reduced.

The temperature of the substrate is mainly determined by the thermal evolution undergone by the coating while degrading. Thus, volatile release and swelling cause a significant reduction in the rate of temperature increase for a certain time interval ($t_d = 116$ s, Figure 3). The contribution given by swelling to the delay in the substrate heating rate is the most important feature derived from the use of intumescent coatings. This delay also causes a retardancy is unwanted reactions, when intumescent coatings are used to protect explosives or highly reactive systems, thus increasing the escape time. For instance, for fires in aircraft carriers, weapons make the risk particularly high in terms of human life and economic damage (Anderson and Wauter, 1984)) and an improvement in "cook-off" (detonation caused by reaction exothermicity even if external heat sources are removed) is very important. Indeed, under fire conditions, after certain transients, the substrate temperature will always attain very high values and burning/explosion cannot be avoided.

Influences of the thermal conductivity model and comparison between predictions and measurements

A comparison is made of predictions from different models of the effective thermal conductivity. They are the model developed by Anderson with the inclusion of the radiative contribution (Eq. 19, Model A), the model developed by Anderson with no radiative heat transfer (Eq. 18, Model B), the model based on the so-called "mixture rule" (Eq. 22, Model C), and the model proposed by Curtis and Miller (1988) (Eq. 23, Model D). Results in terms of the time profiles of substrate temperature and total coating mass fraction (data as in Table 1, reference case) are shown in Figure 6. Parameters characterizing the heating process (d_1, d_2, t_d and t_s) as simulated by Models A–D are reported in Table 2. A comparison between the predictions of Models A and B indicates that the initial heating transients are not affected by radiative heat transfer (about the same values for d_1). On the contrary, radiation highly affects the substrate temperature evolution once charring begins with maximum heating rates becoming

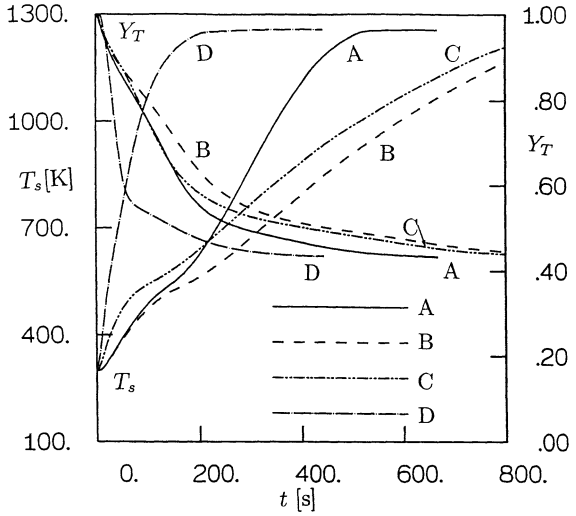

Figure 6. Time profiles of substrate temperature T_s and total coating mass fraction Y_T for different models of the effective thermal conductivity.

Model A (Eq. 19), Model B (Eq. 18), Model C (Eq. 22), and Model D (Eq. 24), and other conditions.

about 2.6 times faster. In the absence of radiation, for times longer than 250 s, the temperature profile becomes linear along the degrading coating thickness (this feature is also shown by Models C and D) and times needed to achieve steady conditions are much longer. The delay in the substrate temperature rise and the swelling time also become longer (factors of about 1.3 and 1.2, respectively). On the whole, the radiative contribution highly affects the heating process once charring begins. Consequently, owing to the presence of spatial temperature gradients along the coating thickness, the intumescent behavior is also influenced. Differences in the coating weight-loss dynamics are also large.

Models C and D do not include any radiative contribution. Hence, their predictions are compared with those of Model B. Model C predicts higher effective thermal conductivities for the virgin coating. Thus, d_1 is about 2 times higher. The faster initial stage also gives rise to shorter delay and swelling times (by factors of about 1.6). Substrate heating becomes extremely fast when Model D is used, so that the intumescent behavior is almost completely missed with a delay about 6 times shorter than that of Model B. For both Models C and D, coating degradation occurs with a faster rate and terminates earlier.

Table 2. Simulation for the Reference Case and Different Models for the Effective Thermal Conductivity

Thermal Conduct. Model	d_1 (K/s)	d_2 (K/s)	t_d (s)	t_s (s)
A, Eq. 19	2.4	2.6	116	151
B, Eq. 18	2.3	1	153	182
C, Eq. 22	5	1	98	113
D, Eq. 24	13	7.6	25.5	25.5

Delay time, t_d; swelling time, t_s, and maximum heating rates of the substrate, d_1, d_2.

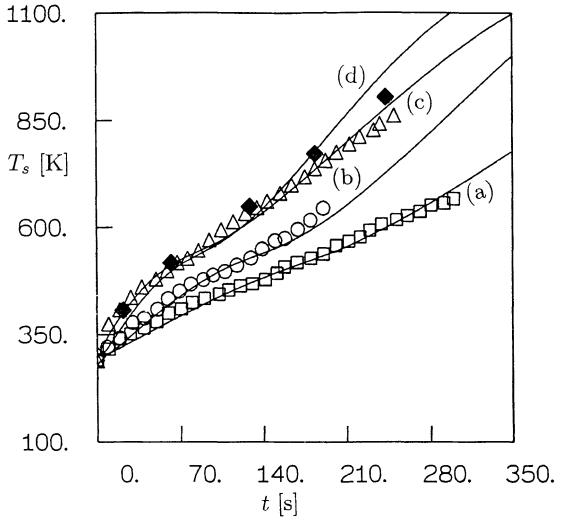

Figure 7. Predicted (solid lines) vs. measured (symbols, Cagliostro et al., 1975) time profiles of the substrate temperature T_s for different conditions.

(a) $Q = 167$ kW/m^2, $\tau_{c0} = 0.2\times10^{-2}$ m, $\tau_s = 0.3\times10^{-2}$ m;
(b) $Q = 157$ kW/m^2, $\tau_{c0} = 0.2\times10^{-2}$ m, $\tau_s = 0.15\times10^{-2}$ m;
(c) $Q = 157$ kW/m^2, $\tau_{c0} = 0.1\times10^{-2}$ m, $\tau_s = 0.15\times10^{-2}$ m;
(d) $Q = 157$ kW/m^2, $\tau_{c0} = 0.15\times10^{-2}$ m, $\tau_s = 0.1\times10^{-2}$ m.

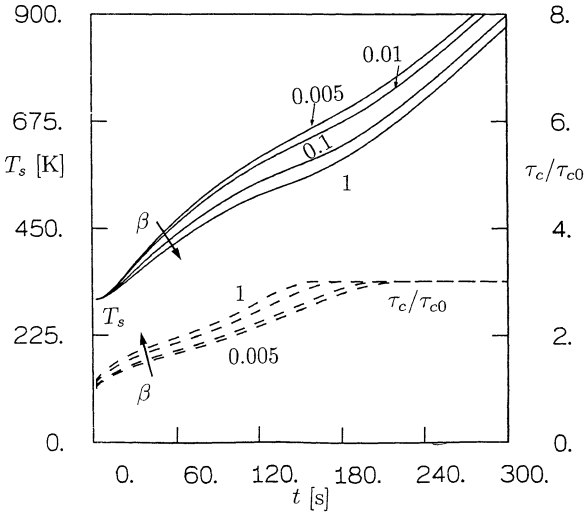

Figure 8. Time profiles of substrate temperature T_s and ratio $\tau_c(t)/\tau_{c0}$ (current to initial coating thickness) for different values of parameter β and other parameters as in Table 1.

The predictions of the thermal response of the coating/substrate system appear to be highly affected by the model of the effective thermal conductivity. Thus, the best model is selected after a comparison with experimental measurements of the time profiles of the substrate temperature (Cagliostro et al., 1975). Figure 7 shows this comparison for the thermal conductivity Model A and the following cases:

(a) $Q = 167$ kW/m^2, $\tau_{c0} = 0.2\times10^{-2}$ m, $\tau_s = 0.3\times10^{-2}$ m,
(b) $Q = 157$ kW/m^2, $\tau_{c0} = 0.2\times10^{-2}$ m, $\tau_s = 0.15\times10^{-2}$ m, (reference case),
(c) $Q = 157$ kW/m^2, $\tau_{c0} = 0.1\times10^{-2}$ m, $\tau_s = 0.15\times10^{-2}$ m,
(d) $Q = 157$ kW/m^2, $\tau_{c0} = 0.15\times10^{-2}$ m, $\tau_s = 0.1\times10^{-2}$ m.

The agreement between measurements and predictions is good. Given the large differences between Model A and the others (Figure 6 and Table 1 refer to case (b)), it can be understood that none of the models B, C and D can be used for quantitative predictions.

Apart from the specification of sample size and applied heat-flux as listed above, the simulations have been obtained with the use of reference data (Table 1) except for case (c) which required a swelling factor of 5 (instead of 3). It is possible that the total coating expansion is dependent on the heating rate. In particular, the model indicates that the effectiveness of the intumescent behavior should improve at high-heating rates (indeed, case (c) considers the thinnest coating). It is also possible that the degradation kinetics obtained under thermogravimetric conditions cannot be extrapolated for high-heating rates. Unfortunately, no experimental information is currently available on these issues. On a global basis, the mathematical formulation of the problem proposed here with Model A for the effective thermal conductivity for the first time predicts quantitatively well the thermal response of the composite system substrate/coating, with no adjustable parameter for slow heating and only the swelling factor for fast heating. Model A is also used for the successive parametric/sensitivity analyses presented in this study.

Influences of swelling and intumescent system thickness

In order to investigate the influences of the bubbling mechanism parameters (β and E) on the process characteristics, a first set of simulations has been made for the reference case with $E = 3$, while β is varied from 1 to 0.005 (lower values give rise to volume expansions below a factor of 3 with respect to the initial value and are not considered). Process dynamics remain qualitatively the same, as discussed above. As expected, the time needed in order to complete coating swelling becomes successively longer as the fraction β is decreased, with variations roughly between 151 and 213 s (Figure 8). As the swelling process becomes slower, the shoulder in the time profile of the substrate temperature tends to disappear, with heating rates becoming slightly higher and the delay time t_d varying from 116 to 142 s (maximum variations of about 20%).

Figure 9, which reports the spatial profiles of the nondimensional (with respect to the initial value) elementary cell size and the degradation rate of the component S_2 for a certain time (25 s) and two widely different values of β (0.1 and 0.005), indicates that the amount of gas retained by the coating during the swelling process is always very small. Indeed, complete expansion occurs for values of the local devolatilization rate of the component S_2 equal to about only 0.5% of the corresponding maximum value (for all β values). Hence, the description of the delay in the release of the gas by each elementary coating cell caused by swelling (variable M_b and Eqs. 15a–15c) is not important (even for expansion factors up to 20) and a simplification in the mathematical model can be introduced. Furthermore, swelling takes place through a zone, whose thickness becomes successively thin-

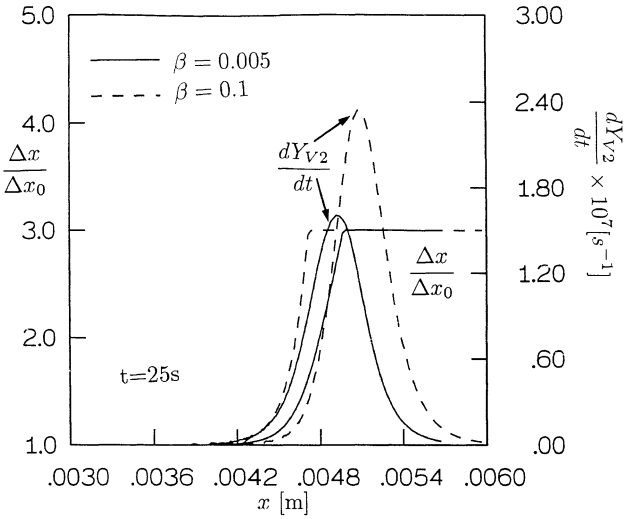

Figure 9. Spatial profiles (for a time of 25 s) of the local devolatilization rate of component S_2, dY_{V2}/dt, and ratio $\Delta x(t)/\Delta x_0$ (current to initial cell size) for $\beta = 0.1$ (dashed lines) and $\beta = 0.005$ (solid lines) and other parameters as in Table 1.

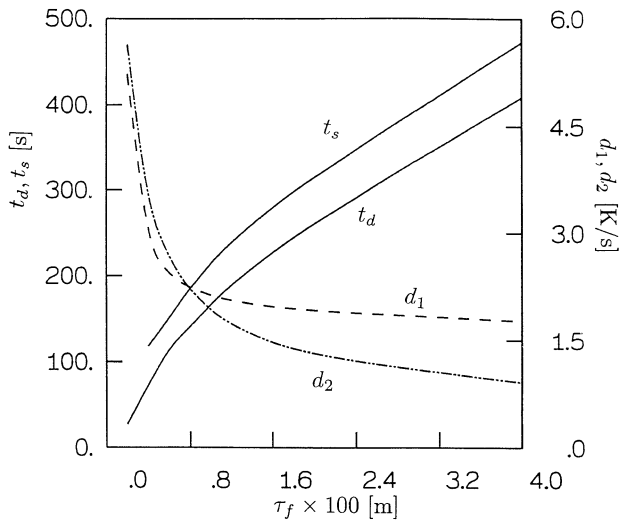

Figure 11. Delay time t_d, swelling time t_s, and maximum heating rates of substrate, d_1, d_2, as functions of final coating thickness τ_f, as obtained by varying the swelling factor E in the range 1—20 and other parameters as in Table 1.

ner as β is increased, rapidly propagating along the virgin coating, as soon as the degradation rate of the component S_2 attains values different from zero. On the whole, for a swelling factor of 3, the process characteristics are only weakly affected by the amount of gas retained by the condensed phase. That is, they are mainly dependent on the initial degradation temperature of component S_2, as postulated in the simplified model developed by Buckmaster et al. (1986). The same considerations apply for the mean molecular weight of volatiles V_2 (Eq. 12).

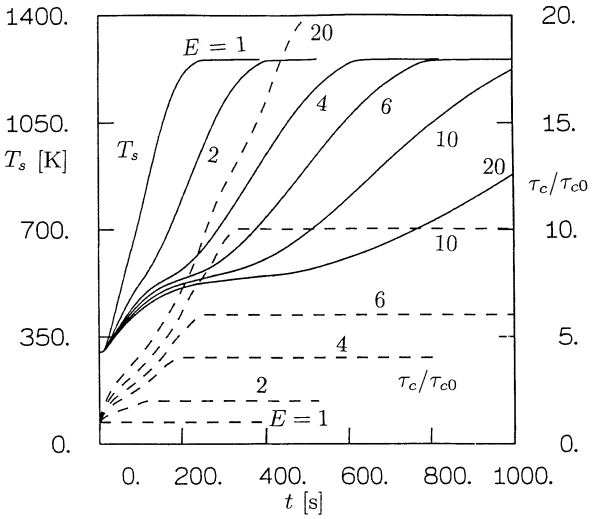

Figure 10. Time profiles of substrate temperature T_s and ratio $\tau_c(t)/\tau_{c0}$ (current to initial coating thickness) for different values of swelling factor E and other parameters as in Table 1.

The influence of the expansion factor E on the process characteristics is investigated for values between 1 (no swelling) and 20 (reference case with $\beta = 1$). Results in terms of time profiles of the substrate temperature and the total coating thickness are reported in Figure 10. As expected, substrate heating becomes successively slower as the expansion factor is increased. In particular, it is worth noting that a small delay in the substrate temperature rise is also observed in the absence of swelling ($E = 1$), as a result of the convective cooling of outflow volatile pyrolysis products and, to a small extent, of the endothermicity of reactions $r1-r2$.

The delay and the swelling times increase with E and, as shown in Figure 11, they present the same qualitative dependence on the final coating thickness, as determined by the range of E factors mentioned above. That is, a first region of strong dependence (final coating thicknesses below $0.6-0.8\times10^{-2}$ m) is followed by a slower increase. Furthermore, for the first zone, d_1 and d_2 attain comparable values, roughly between 5.5 and 2.2 K/s. For large expansion factors, maximum heating rates of the substrate are attained during the initial stage (d_1) and are almost independent of the swelling process.

The effects of variations in the initial coating thickness on the heating characteristics of the substrate are qualitatively similar to those caused by the swelling factor. However, as appears from Figure 12, the delay and the swelling times present an almost linear dependence on the final coating thickness, as simulated for different τ_{c0} values ($0.05-0.4\times10^{-2}$ m and $E = 3$). In addition, while values are comparable for small final thicknesses (below 0.6×10^{-2} m), irrespective of variations in E or τ_{c0}, variations in the initial coating thickness are, by far, more effective for high final coating thicknesses. In other words, convective cooling due to coating devolatilization (and, probably, to coating thermal inertia) plays

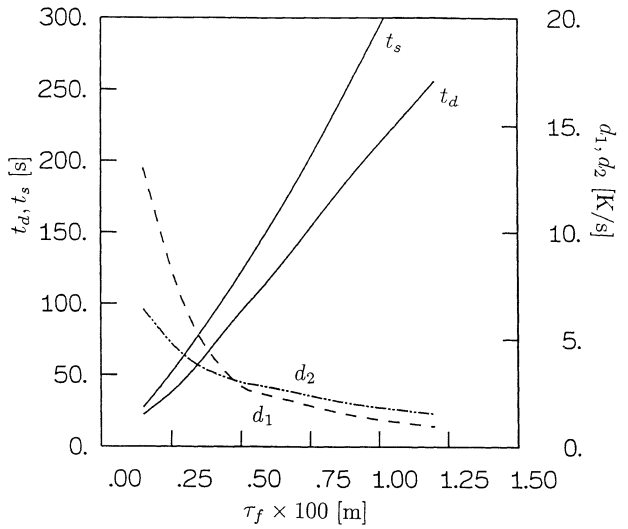

Figure 12. Delay time t_d, swelling time t_s, and maximum heating rates of substrate, d_1, d_2, as functions of the final coating thickness τ_f, as obtained by varying the initial coating thickness in the range $0.05–0.4\times10^{-2}$ m ($E=3$) and other parameters as for the reference case.

an important role for the time evolution of the substrate temperature. Again, the heating rates of the substrate decrease as the coating thickness increases, with maxima observed at the beginning of the degradation process (d_1) for thin samples (low thermal inertia) and during the final stage (d_2) for thicker samples (due to radiative heat transfer).

In general, the intumescent behavior is successively more effective as swelling occurs to a successively larger extent. Also, the role of factor E is more important than that of factor β. For a final given thickness of the coating, the effects of the initial coating thickness are higher in terms of thermal protection than those associated with the swelling factors, due essentially to enhanced convective cooling. Finally, the size, and, presumably, the properties of the material being protected, are also important in relation to its thermal behavior. For instance, the delay time increases linearly with the substrate mass (simulations made by varying the substrate thickness, not shown).

Sensitivity analysis

In order to assess the influences of physical properties and kinetic constants on the predictions of the thermal response of the substrate, a sensitivity analysis is carried out. A sensitivity parameter (Di Blasi, 1993, 1997) is introduced, defined as the ratio between the % of the deviation of outputs (the + and − signs indicate an increase and decrease from the reference value, respectively) to the % deviation of inputs (again with respect to the reference value). Deviations of $\pm20\%$ have been considered for all the input parameters. Reference values of the output variables are those predicted by means of the input data listed in Table 1. Output variables examined include the two local maxima in the time profile of the substrate temperature (d_1 and d_2) and the delay time t_d.

Table 3. Sensitivity of Outputs, d_1, d_2 and t_d, to Coating Properties*

Parameter	d_1 (%)	d_2 (%)	t_d (%)
$ef+$	0	0.17	0
$ef-$	0	0.17	0
$df+$	0	0.47	0
$df-$	0	0.26	0
$\epsilon_{c0}+$	−0.377	0	−0.300
$\epsilon_{c0}-$	−0.566	0	−0.330
$\rho_{c0}+$	−0.377	−0.260	0.487
$\rho_{c0}-$	−0.471	−0.086	0.302
$\tau_{c0}+$	−1.180	−0.400	1.460
$\tau_{c0}-$	−0.370	−0.700	1.030
$E+$	0.280	−0.820	0.836
$E-$	−1.368	−0.776	1

*Sensitivity is the ratio between the % of the deviation of outputs, with respect to the reference values, to $\pm20\%$ deviation of inputs, again with respect to reference values.

In practice, no sensitivity is shown for variations in the specific heats (c_c and c_f), the thermal conductivity (λ_{c0}), the emissivity (e_{c0}), the initial pore diameter (d_{c0}), the swelling parameter β, the V_2 molecular weight W_{V2}, the reaction heats Δh_k, $k=1$, 3, or the preexponential factors of reactions $r1$, $r2$. Results for other physical properties and model parameters are reported in Table 3 and for kinetic constants in Table 4.

Variables which contribute to the definition of the effective thermal conductivity (Eq. 19) e_f, d_f, ϵ_{c0} mainly influence the substrate heating rate. As expected, variations in the char emissivity and final pore diameter of char slightly affect the characteristics of the final heating stage (d_2). On the other hand, variations in the initial coating porosity mainly affect the initial heating rate (d_1) and, to a small extent, the delay time.

The sensitivities are comparatively higher for variables related to the size of the coating (τ_{c0} and E) and the total volatile mass evolved (ϱ_{c0}). The dependence of the process characteristics on the initial coating thickness and the model parameter E has already been discussed. It is worth noting that this analysis confirms that the highest sensitivity is for the initial coating thickness (higher final thickness and higher amounts of volatile mass released).

From the results shown in Table 4, it appears that E_1 exerts only a small influence on the initial process transients. The sensitivity in the parameter E_2 is high, and an increase

Table 4. Sensitivity of Outputs d_1, d_2 and t_d to Kinetic Constants*

Parameter	d_1(%)	d_2(%)	t_d(%)
E_1+	0.14	0	0
E_1-	0.47	0	0
E_2+	1.51	−0.387	0.877
E_2-	1.79	−0.302	1.320
A_3+	0	0.258	0
A_3-	0	0.258	0
E_3+	0.047	−1.465	1.030
E_3-	−0.283	−1.980	0.930

*Sensitivity defined as in Table 3.

causes a delay in the swelling process. Consequently, heating rates of the substrate are faster in the initial stage (d_1) and slower in the final stage (d_2). The delay in the heating process is highly dependent on this parameter and, in general, it becomes significantly longer (the contrary occurs for a decrease in E_2). High process sensitivity is also observed for variations in E_3. As this is decreased (with respect to the reference value), the solidification (charring) stage becomes faster and, given the enhanced heat transfer due to pore radiation, the delay time becomes shorter and the heating rate in the final stage becomes faster (for variations of 20%, sensitivity to the activation energies is higher than that of preexponential factors, given their exponential dependence on a key variable, that is, temperature).

Conclusions

This study has presented a mathematical model, comprehensive of the description of the main processes occurring during the degradation of intumescent coatings. A finite-difference formulation of the conservation equations has been derived for a variable volume system. The occurrence of swelling is associated with the beginning of the degradation of one of the three coating components. Although the treatment proposed requires two empirical parameters, namely the fraction of gas retained by the degrading medium and the expansion factor, it is only the second parameter which plays a dominant role in the decomposition dynamics and the substrate heating characteristics.

The process characteristics are highly dependent on the model applied for the effective thermal conductivity. Literature models have been compared and it has been found that only a model specifically developed for intumescent coatings (Anderson et al., 1988), extended to include a radiative contribution (Di Blasi, 1996a), correctly predicts from both the qualitative and the quantitative point of view the time evolution of the substrate temperature. Note that none of the models which previously appeared in the literature has accomplished this goal.

Examination of the substrate temperature profile, for high external heat fluxes reproducing fire conditions, reveals that three main regions exist. The first reports a rapid temperature rise, whose characteristics are essentially determined by the virgin coating properties. The second is a delay in the temperature rise, caused by coating decomposition (release of hot volatile species) and swelling (volume expansion and high void fraction). The characteristics of this zone are mainly affected by the initial coating thickness and density, and the expansion. The third zone corresponds to coating charring and heat transfer dominated by the radiative contribution in the effective thermal conductivity.

A sensitivity analysis, carried out to evaluate the importance of a reliable knowledge of coating physical properties, indicates that the dominant parameters are the size (initial and final thickness) and the density, which can be easily measured. The kinetic constants (decomposition mechanism) also present high sensitivities and, thus, should be carefully determined, in particular, those associated with volatile release responsible for swelling and charring. The initiation of the latter process is also important in relation to the mechanism of radiative heat transfer, which controls the thermal evolution of the substrate in the final stage. On the whole, although a high number of input parameters are required by the transport model of coating decomposition presented here, the sensitivity is high only for a few of them.

Extensive experimental research is needed in relation to degradation mechanisms of intumescent materials and measurements of variables (coating and substrate temperature profiles, volatile mass flux, gas composition, and so on) under practical conditions (heat- and mass-transfer control). Results will give the means for further process understanding, and will provide information for the application of mathematical models in the fields of material design and advanced fire protection technologies. Finally, a more rigorous mathematical description of the thermal response of intumescent systems should be developed, taking into account the rheological behavior of the material (properties and their variation with reaction conditions, and transport phenomena with a more accurate treatment of bubble dynamics).

Notation

A = cross section of the substrate/coating system, m^2
A_1, A_2, A_3 = pre-exponential factors, s^{-1}
c = heat capacity, kJ/kg·K
d_c = pore diameter of coating, m
d_f = pore diameter of char, m
d_1, d_2 = maximum substrate heating rates (initial and final stage), K/s
E = volume expansion factor
E_1, E_2, E_3 = activation energies, kJ/mol
e = surface emissivity
h = convective heat-transfer coefficient, kW/m^2·K
K = reaction rate constant, s^{-1}
M_0 = initial mass of each elementary volume, kg
N = diffusive mass flux, kg/m^2·s
n = number of elementary cells in the coating finite-difference approximation
n_b = number of time steps needed to attain the maximum volume expansion
p_0 = gas-phase pressure, N/m^2
Q = external heat flux, kW/m^2
q = conductive heat flux, kW/m^2
$\mathfrak{R}$ = universal gas constant, kJ/mol·K
T = coating temperature, K
T_f = coating temperature at the irradiated surface, K
T_s = substrate temperature, K
t = time, s
t_d = delay time, s
t_s = swelling time, s
u = gas velocity, m/s
V = volume, m^3
W = convective flux, kg/m^2·s
W_g = gas mean molecular weight, kg/mol
W_{V2} = molecular weight of species V_2, kg/mol
x = spatial coordinate, m
Y_1, Y_2, Y_3, Y_C = species mass fraction
Y_T = total coating mass fraction
β = fraction of volatiles V_2 retained by coating during swelling
Δ_b = bubble volume per unit surface, m
Δh = decomposition heat, kJ/kg
Δ_{ls} = solid volume per unit area, m
Δt = time step, s
Δx = total volume per unit surface (cell size along the x direction), m
ϵ = porosity
λ = thermal conductivity, kW/m·K
ν = stoichiometric coefficient
ρ = gas density, kg/m^3

σ = Stefan-Boltzmann constant, kW/m$^2\cdot$K^4
ω = pore emissivity
τ = thickness, m

Subscripts

b = bubble
C = char species
c = coating
e = external
f = final (char)
g = volatiles
i = elementary volume
ls = condensed phase
s = substrate
T = total mass fractions referred to the total coating mass
0 = initial or reference conditions
S_1, S_2, S_3 = condensed-phase species
V_1, V_2, V_3 = volatile species
$*$ = effective properties

Acknowledgment

The research was funded in part by the Italian Space Agency (ASI) under the Contract I/R/102/00.

Literature Cited

Anderson, C. E., and D. K. Wauters, "A Thermodynamic Heat Transfer Model for Intumescent Systems," *Int. J. Eng. Sci.*, **22**, 881 (1984).

Anderson, C. E., D. E. Ketchum, and W. P. Mountain, "Thermal Conductivity of Intumescent Chars," *J. of Fire Sci*., **6**, 390 (1988).

Buckmaster, J., C. Anderson, and A. Nachman, "A Model for Intumescent Paint," *Int. J. of Eng. Sci*., **24**, 263 (1986).

Cagliostro, D. E., S. R. Riccitello, K. L. Clark, and A. B. Shimizu, "Intumescent Coating Modelling," *J. of Fire & Flammability*, **6**, 205 (1975).

Camino, G., L. Costa, and L. Trossarelli, "Study of the Mechanism of Intumescence in Fire Retardant Polymers: II. Mechanism of Action in Polypropylene-Ammonium Polyphosphate-Pentaerithritol Mixture," *Poly. Deg. and Stab*., **7**, 25 (1984).

Carslaw, H. S., and J. C. Jaeger, *Conduction of Heat in Solids*, 2nd ed., Oxford University Press, Oxford (1980).

Collins, R. E., *Flow of Fluids Through Porous Materials*, Reinhold Publ., New York (1961).

Curtis, L. J., and D. J. Miller, "Transport Model with Radiative Heat Transfer for Rapid Cellulose Pyrolysis," *Ind. Eng. Chem. Res*., **27**, 1775 (1988).

Di Blasi, C., "Analysis of Convection and Secondary Reaction Effects within Porous Solid Fuels Undergoing Pyrolysis," *Comb. Sci. and Tech*., **90**, 315 (1993).

Di Blasi, C., and I. S. Wichman, "Effects of Solid Phase Properties on Flames Spreading over Composite Materials," *Comb. and Flame*, **102**, 229 (1995).

Di Blasi, C., "Heat, Momentum and Mass Transfer through a Shrinking Biomass Particle Exposed to Thermal Radiation," *Chem. Eng. Sci*., **51**, 1121 (1996a).

Di Blasi, C., "Modeling of Solid and Gas Phase Processes during Composite Material Degradation," *Poly. Degrad. and Stab*., **54**, 241 (1996b).

Di Blasi, C., "Influences of Physical Properties on Biomass Devolatilization Characteristics," *Fuel*, **76**, 957 (1997).

Di Blasi, C., "The State of the Art of Transport Models for Charring Solid Degradation," *Poly. Int*., **49**, 1133 (2000a).

Di Blasi, C., "Dynamic Behaviour of Stratified Downdraft Gasifiers," *Chem. Eng. Sci*., **55**, 2931 (2000b).

Ellard, J. A., "Performance of Intumescent Fire Barriers," *ACS Org. Coatings and Plastics*, **33**, 531 (1973).

Horrocks, A. R., "Development in Flame Retardants for Heat and Fire Resistant Textiles—The Role of Char Formation and Intumescence," *Poly. Degrad. and Stab*., **54**, 143 (1996).

Kandola, B. J., S. Horrocks, and A. R. Horrocks, "Evidence of Interaction in Flame-Retardant Fiber-Intumescent Combinations by Thermal Analytical Techniques," *Thermochimica Acta*, **294**, 113 (1997).

Le Bras, M., G. Camino, S. Bourbigot, and R. Delobel, Eds., *Fire Retardancy of Polymers—The Use of Intumescence*, The Royal Society of Chemistry, Cambridge, U.K. (1998).

Lewin, M., "Physical and Chemical Mechanisms of Flame Retarding of Polymers," *Fire Retardancy of Polymers—The Use of Intumescence*, Le Bras et al., eds., The Royal Society of Chemistry, Cambridge, U.K., p. 3 (1998).

Mameleev, V. S., and K. M. Gibov, "Modelling Fire Retardant Intumescent Polymeric Materials," in *Fire Retardancy of Polymers: The Use of Intumescence*, M. Le Bras, et al., eds., The Royal Society of Chemistry, Cambridge, U.K., p. 113 (1998).

Patankar, S. V., *Numerical Heat Transfer and Fluid Flow*, Hemisphere Publishing Corp., New York (1980).

Siat, C., M. Le Bras, and S. Bourbigot, "Combustion Behaviour of Ethylene Vinyl Acetate Copolymer-Based Intumescent Formulations Using Oxygen Consumption Calorimetry," *Fire and Materials*, **22**, 119 (1998).

Yanenko, N. N., *The Method of Fractional Steps*, Springer-Verlag, New York (1971).

Yang, J., P. A. Tanguy, and C. Roy, "Heat Transfer, Mass Transfer and Kinetic Study of the Vacuum Pyrolysis of a Large Used Tire Particle," *Chem. Eng. Sci*., **50**, 1909 (1995).

Wichman, I. S., "On the Use of Operator-Splitting Methods for the Equations of Combustion," *Combustion and Flame*, **83**, 240 (1991).

Weil, E. D., W. Zhu, N. Patel, and S. M. Mukhupadhyay, "A System Approach to Flame Retardancy and Comments on the Mode of Action," *Poly. Degrad. and Stab*., **54**, 125 (1996).

Manuscript received July 3, 2000, and revision received Mar. 2, 2001.